Strain-sensitive spin-state ordering in thin films of perovskite $LaCoO_3$

J. Fujioka,[1] Y. Yamasaki,[1,2,3] A. Doi,[1] H. Nakao,[2] R. Kumai,[2] Y. Murakami,[2]
M. Nakamura,[3] M. Kawasaki,[1,3] T. Arima,[3,4] and Y. Tokura[1,3]

[1]*Department of Applied Physics and Quantum-Phase Electronics Center (QPEC), University of Tokyo, Hongo, Tokyo 113-8656, Japan*
[2]*Condensed Matter Research Center (CMRC) and Photon Factory, Institute of Materials Structure Science (IMSS), High Energy Accelerator Research Organization (KEK), Tsukuba, 305-0801, Japan*
[3]*RIKEN Center for Emergent Matter Science (CEMS), Wako 351-0198, Japan*
[4]*Department of Advanced Materials Science, University of Tokyo, Kashiwa 227-8561 Japan*

(Received 9 May 2015; revised manuscript received 23 August 2015; published 9 November 2015)

We have investigated the lattice distortion coupled to the Co $3d$-spin-state ordering in thin films of perovskite $LaCoO_3$ with various epitaxial strains by measurements of the magnetization, x-ray diffraction, and optical spectra. In the system with tensile strain about 0.5%, a lattice distortion characterized by the modulation vector $q = (1/6,1/6,1/6)$ emerges at 40 K, followed by a ferromagnetic ordering at 24 K. Alternatively, in systems with tensile strain exceeding 1%, the lattice distortion characterized by $q = (1/4,1/4,1/4)$ emerges at 120 K or higher, and subsequently the ferromagnetic or ferrimagnetic ordering occurs around 90 K. The evolution of infrared phonon spectra and resonant x-ray scattering at the Co K edge suggests that the population change in the Co $3d$ spin state causes the strain-induced switching of spin-state ordering as well as of magnetic ordering in this canonical spin-state crossover system.

DOI: 10.1103/PhysRevB.92.195115 PACS number(s): 75.25.Dk, 75.70.−i, 78.30.−j, 78.70.Ck

I. INTRODUCTION

The spin-state transition in solids offers fertile ground to yield unique optical, magnetic, elastic, and thermoelectric phenomena via the interplay among charge, spin, and orbital degrees of freedom. For example, thermally- or photoinduced nonmagnetic-paramagnetic transitions have been extensively studied in a variety of materials including organometallic complex or transition-metal oxides for these decades [1,2]. The perovskite $LaCoO_3$ is one of the canonical spin-state crossover materials which exhibits a thermally induced nonmagnetic-paramagnetic crossover as well as an insulator-metal crossover [3–13]. In this system, the nominally trivalent Co-ion (Co^{3+}) forms the three-dimensional network with corner-sharing CoO_6 octahedra and may take three different spin states: the low-spin (LS) state with filled $3d$ t_{2g} manifold ($S = 0$), intermediate-spin (IS) state with active e_g and t_{2g} orbital degrees of freedom ($S = 1$), and high-spin (HS) state with active t_{2g} orbital degree of freedom ($S = 2$), as shown in Fig. 1(a). Specifically, a thermally induced crossover from nonmagnetic to paramagnetic state is observed around 90 K. The system remains semiconducting upon this spin-state transition but gradually turns into a metallic state above 600 K. It is recognized that the nonmagnetic-paramagnetic crossover is attributed to the change in the Co−$3d$ spin state from a LS state to a IS or HS state, but the specific model of spin state in the paramagnetic state has remained elusive [3–14].

The spin-state transition is also triggered by the application of epitaxial strain in samples of thin film form. In thin films with the tensile strain, a ferrimagnetic or ferromagnetic ordering emerges at low temperatures instead of the nonmagnetic ($S = 0$) state while keeping an insulating behavior [15–18]. This is in contrast with the bulk system, in which the low-temperature nonmagnetic state is robust in a series of $RCoO_3$ (R = rare earth) as shown in Fig. 1(b). Recent research has uncovered that the unique ordering of Co − $3d$ orbitals in the IS and/or HS-state plays an essential role for the ferrimagnetic/ferromagnetic ordering [19–22]. One of the characteristic features of orbital ordering is the high susceptibility to the lattice distortion. Indeed, it has been demonstrated that the tuning of epitaxial strain causes the dramatic change in the electronic/magnetic properties via the modulation of orbital ordering in perovskite manganese oxides [23]. The tuning of epitaxial strain may modify the ferrimagnetic or ferromagnetic ordering in the present system via the change in the spin-state ordering, yet this has not been experimentally demonstrated. In this study, we have investigated the magnetization and lattice distortion in the epitaxial thin films of $LaCoO_3$ grown on various substrates with different lattice constants and crystal orientations, focusing on the evolution of magnetic and spin-state ordering with tuning of the epitaxial strain. We found that the lattice distortion characterized by the modulation vector $q = (1/6,1/6,1/6)$ emerges at 40 K, followed by a ferromagnetic ordering at 24 K in the weakly strained thin film (∼0.5%). Alternatively, in moderately strained systems ($\gtrsim$%), the lattice distortion characterized by $q = (1/4,1/4,1/4)$ emerges at 120 K or higher, and subsequently the ferromagnetic or ferrimagnetic ordering emerges around 90–92 K. Combined with the results of infrared optical spectra and resonant x-ray diffraction, we discuss the possibility that the population change in the strain-induced spin state is responsible for the evolution of the spin-state ordering as well as the magnetic ordering.

II. EXPERIMENTAL

Single crystalline films of $LaCoO_3$ were fabricated on the $(LaAlO_3)_{0.3}(SrAl_{0.5}Ta_{0.5}O_3)_{0.7}$ (LSAT) substrate with (111) and (001) orientation and the $SrTiO_3$ substrate with (111) orientation by the pulsed laser deposition technique. The crystal orientations on these substrates are schematically shown in Fig. 1(c). Figures 2(a), 2(b), and 2(c) show the reciprocal space mapping around (112), (103), and (112) fundamental reflections for films on LSAT(111), LSAT(001),

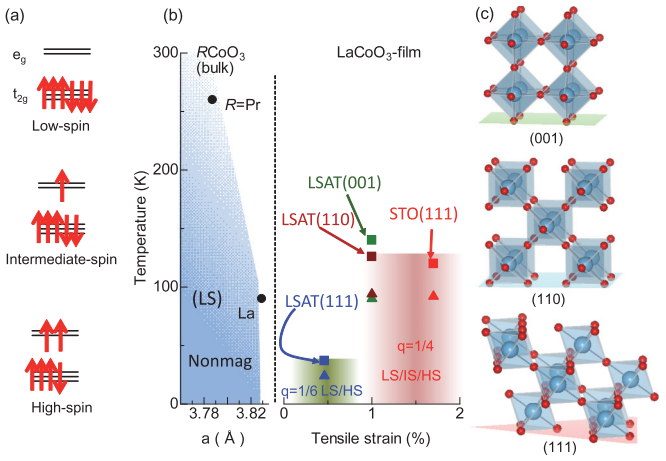

FIG. 1. (Color online) (a) Schematic view of the spin states of trivalent Co-ion (Co^{3+}): the low-spin (LS), intermediate-spin (IS) and high-spin (HS) states. The arrows denote the electron spins. (b) Phase diagram of the spin-state ordering for tensile strained $LaCoO_3$ thin film as well as that of bulk $RCoO_3$ (R: rare earth element), which are distinguished by a vertical dashed line. The circle indicates the typical temperature of crossover from nonmagnetic (NM) to paramagnetic (PM) state as determined by the linear thermal expansion [9]. The squares and triangles denote the transition temperatures of spin-state ordering and those of ferrimagnetic (Ferri) or ferromagnetic (Ferro) ordering, respectively. q is the modulation vector of lattice distortion due to the spin-state ordering. The lattice constant (a) is defined as the cubic root of the unit cell volume in the pseudocubic setting. (c) Schematic view of the crystal structure for the thin film of $LaCoO_3$ grown on substrates with (001), (110), and (111) orientations.

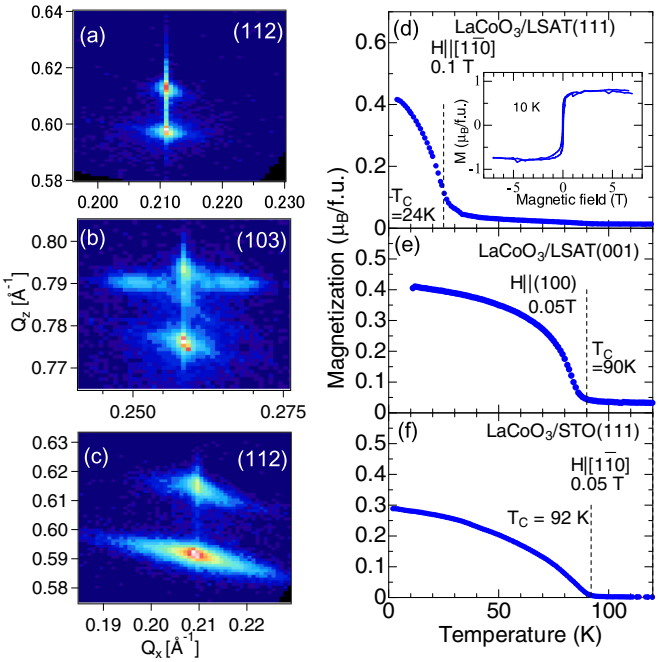

FIG. 2. (Color online) (a)–(c) X-ray reciprocal space mapping around LSAT(112), LSAT(103) and STO(112) reflections and (d)–(e) temperature dependence of the magnetization for $LaCoO_3$ thin films grown on LSAT(111), LSAT(001), and STO(111) substrates, respectively. The inset to (d) shows the magnetization curve of $LaCoO_3$/LSAT (111) at 10 K.

and STO(111), respectively. The horizontal peak positions of the film are coincident with those of substrates, showing that the films were grown coherently while keeping the identical in-plane lattice constants with those of the substrate. On the basis of x-ray diffraction pattern, the magnitude of averaged epitaxial strain, which is derived from the cubic root of the unit cell volume, is estimated to be 0.5%, 1%, and 1.7%, and the film thickness is estimated to be around 60, 38, and 35 nm for the films grown on LSAT(111), LSAT(001), and STO(111) substrates, respectively. Measurements of magnetization were performed by using a SQUID magnetometer. The synchrotron-radiation x-ray diffraction was performed at BL-3A and BL-4C, Photon Factory of KEK, Japan. We measured optical reflectivity spectra between room temperature and 10 K with linearly polarized light using a Fourier transform spectrometer (grating-type monochromator equipped with a microscope) in the photon energy region of 0.008–0.7 eV (0.5–5 eV), respectively. The reflectivity spectra in the energy region of 4–30 eV were measured at room temperature with the use of synchrotron radiation at UV-SOR, Institute for Molecular Science, Japan. We calculated the optical conductivity spectra by means of Kramers-Kronig analysis for the bilayer model [24]; the optical conductivity spectra of films were numerically evaluated, taking into account the multiple reflections at the film-substrate interface.

III. RESULTS AND DISCUSSION

Figures 2(d), 2(e), and 2(f) show the temperature dependence of magnetization for $LaCoO_3$ thin films grown on LSAT(111), LSAT(001), and STO(111) substrates, respectively. For $LaCoO_3$/LSAT(111), the magnetization steeply increases below 24 K (= T_C), suggesting the onset of ferromagnetic or ferrimagnetic ordering. The inset to Fig.2(d) shows the magnetic field dependence of magnetization. The saturated magnetization is estimated to be about 0.7 μ_B/f.u. Alternatively, for $LaCoO_3$/LSAT(001) and $LaCoO_3$/$SrTiO_3$(111), the onset temperature of magnetization is enhanced to 90 K and 92 K. The saturated magnetization is about 0.5–0.9 μ_B/f.u. (data not shown) for both samples, which is comparable to that for $LaCoO_3$/LSAT(111). A similar temperature profile of magnetization has already been reported in previous studies [15–18,22]. Such a significant change in the magnetic transition temperature upon tuning the epitaxial strain suggests that the magnetic structure and underlying spin-state ordering are extremely sensitive to the direction or magnitude of epitaxial strain [25,26].

Then we explored the spatial modulation of lattice distortion by means of the synchrotron-radiation x-ray diffraction. First, we argue the results for the case of $LaCoO_3$/LSAT(111). Figure 3(a) displays the temperature dependence of out-of-plane lattice constant (d_{111}). Here, we adopted the pseudocubic setting for denoting the crystal axes. As temperature decreases, d_{111} monotonically decreases at high temperatures above 50 K but increases below 40 K. Moreover, we have identified superlattice reflections characterized by the modulation vector $q = (1/6, 1/6, 1/6)$ at low temperatures. Figures 3(d) and 3(b) show typical profiles of superlattice reflection and its intensity plotted as a function of temperature, respectively. The scattering intensity of superlattice reflection is steeply enhanced

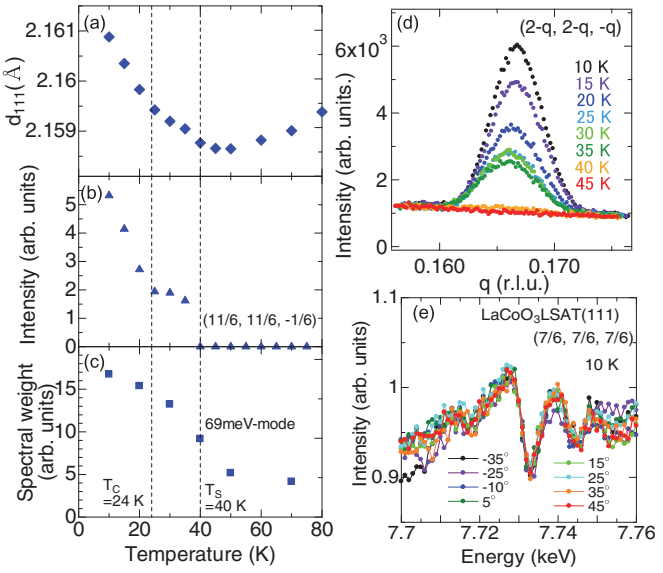

FIG. 3. (Color online) Temperature dependence of (a) out-of-plane lattice constant d_{111}, (b) scattering intensity of superlattice reflection at (11/6, 11/6, −1/6), and (c) spectral intensity of the Co-O stretching optical phonon. (d) Profiles of superlattice reflection at (11/6, 11/6, −1/6) measured at 12 keV. (e) Energy dependence of resonant intensity at (7/6, 7/6, 7/6) reflection. ψ denotes the azimuthal angles around the [111] direction (see also text for definition).

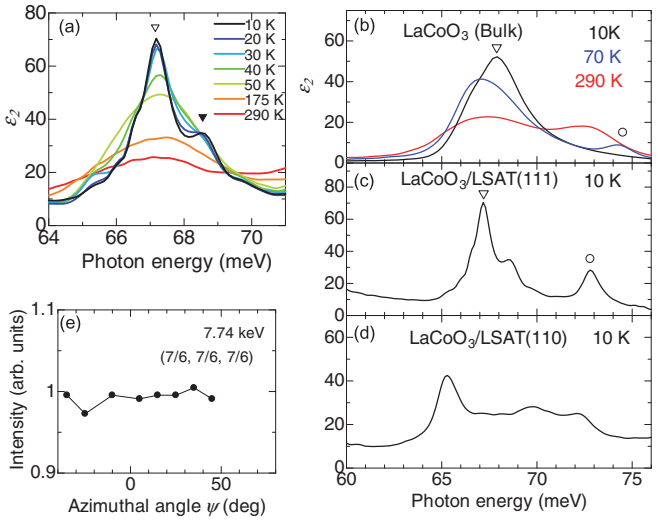

FIG. 4. (Color online) (a) Energy spectra of imaginary part of the dielectric constant (ϵ_2) for the Co-O bond stretching phonon. The peak structure marked by open (closed) triangles denotes the mode at 67 meV (69 meV). (b)–(d) The ϵ_2 spectra of Co-O bond stretching phonon for bulk crystal thin films grown on LSAT(111) and LSAT(110), respectively. The peak structure marked by triangles (circles) denote the main (satellitelike) Co-O stretching mode. (e) Scattering intensity of (7/6, 7/6, 7/6) reflection at 7.74 keV plotted as a function of ψ.

below 40 K (= T_S), suggesting the presence of a structural phase transition; the unit cell is sextuplicated in all [100], [010], and [001] directions accompanying the elongation of lattice constant along the [111] direction. Figure 3(e) shows the scattering spectrum of (7/6, 7/6, 7/6) superlattice reflection around the Co K edge ($1s - 4p$ intra-atomic dipole transition) at various azimuthal angles (ψ). The scattered x-ray includes both σ' and π' polarization components, while the incident x-ray is nearly σ polarized. Here, the σ and π denote the x-ray polarization component perpendicular and parallel to the scattering plane, respectively. The ψ is defined as zero, when the incident x-ray polarization is parallel to the [11$\bar{2}$] direction. The scattering spectrum exhibits a clear resonance structure at the Co K edge around 7.73 keV, suggesting that the lattice modulation accompanies the change in the local crystal/electronic symmetry around Co ions. To get further insight into the structural phase transition, we have investigated anomalies of lattice dynamics via infrared spectra. Figure 4(a) shows the spectra of imaginary part of dielectric constant $\epsilon_2(\omega)$ for optical phonon modes. At 10 K, two Co-O bond stretching modes are discernible at 67 and 69 meV, respectively, whereas the latter gradually smears out with increasing temperature. Such an activation of optical phonon at the low temperature phase may originate from the folding of the Brillouin zone due to lattice modulation. To quantify the evolution of spectral intensity, we fitted the spectra with the Lorentz oscillator model as follows:

$$\epsilon_2(\omega) = \sum_{i=1,2} \frac{S_i \omega_i^2 \gamma_i \omega}{\left(\omega^2 - \omega_i^2\right)^2 + \omega_i^2 \gamma_i^2}.$$

Here, S_i is the oscillator strength, ω_i the mode frequency, and γ_i the damping rate of the ith oscillator; $i = 1,2$ corresponds to the modes at 67 and 69 meV, respectively. We define $S_i\omega_i^2$ as the spectral intensity of the ith oscillator. Figure 3(c) shows the temperature dependence of spectral intensity of the Co-O stretching mode at 69 meV. The spectral intensity markedly increases below T_S, whereas finite intensity appears to subsist even above T_S. It is recognized that the Co-O stretching phonon is sensitive to the Co3d - O2p bond covalency and thus is sometimes utilized as a good probe for the Co-3d spin state [27]. Indeed, such an anomaly of the Co-O stretching phonon has already been observed in the bulk system. Figure 4(b) shows the $\epsilon_2(\omega)$ spectrum for the bulk crystal at various temperatures. A satellitelike Co-O stretching mode emerges around 74 meV in the vicinity of nonmagnetic-paramagnetic crossover around 70 K. The peak intensity is enhanced at higher temperatures, whereas the intensity of original mode is rather reduced. This satellitelike mode is attributed to the dynamical lattice distortion due to the thermally activated IS-state sites or HS-state sites [27]. We note that the spectral shape of Co-O stretching phonons for $LaCoO_3$/LSAT(111) resembles that for bulk crystal at 70 K rather than the fully paramagnetic state at 290 K. This suggests that the spatially averaged spin state in $LaCoO_3$/LSAT(111) is close to that at the initial stage of nonmagnetic-paramagnetic crossover in the bulk system; the IS-state or HS-state sites dilutely populate within the matrix of LS-state sites even at 10 K.

On the basis of these results, we consider the origin of the observed structural phase transition. It has been well recognized that thin films of perovskite oxides often show lattice modulations of various origins such as the strain-induced tilts or rotations of the metal-oxygen octahedra, ferroelectricity, ionic defect ordering, and charge/orbital ordering. Indeed,

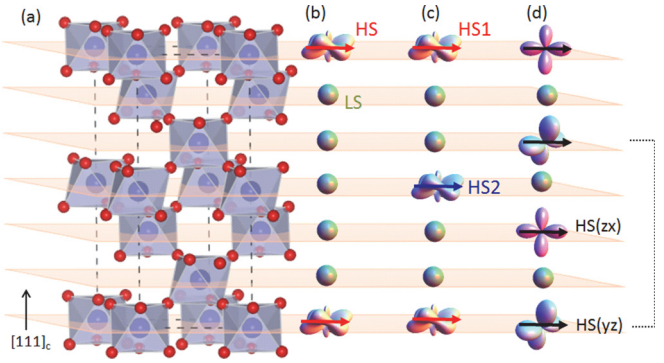

FIG. 5. (Color online) (a) Crystal structure of $LaCoO_3$ with the rhombohedral symmetry. Dashed lines indicate the unit cell. Note that the [001] axis in the rhombohedral setting corresponds to the [111] axis in the pseudocubic setting. (b) Schematic view of spin-state ordering including the low-spin (LS) state sites and high-spin (HS) state sites. The lobes exemplify the $|j_{\rm eff} = 1, j_z = \pm 1\rangle$ state of the HS-state. Spheres represent the LS-state sites with fully occupied t_{2g} manifold. The ordered spins are denoted with arrows. (c) Schematic view of spin-state ordering including the LS-state site and two inequivalent HS-state sites. (d) An example of spin and orbital ordering with the modulation vector (1/4, 1/4, 1/4). The dashed line indicates the one unit of superstructure (four sites along the [111] direction).

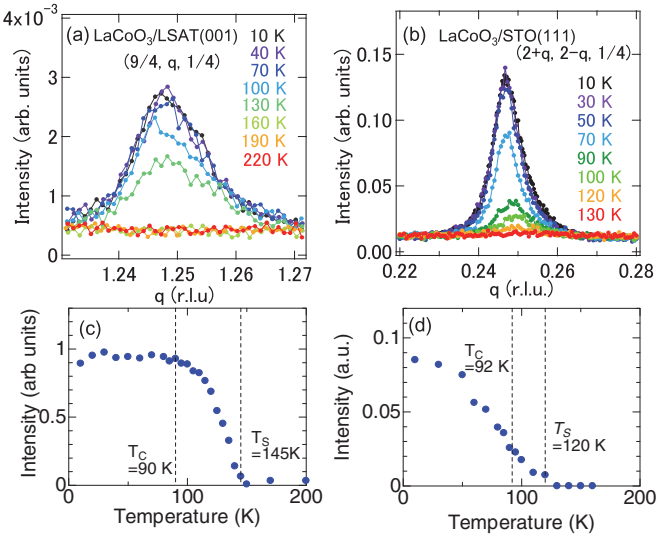

FIG. 6. (Color online) Profiles of superlattice reflection (a) around (9/4, 5/4, 1/4) in $LaCoO_3$/LSAT(001) and (b) around (9/4, 7/4, 1/4) in $LaCoO_3$/STO(111). The measurements were performed at the nonresonant condition (incident x-ray photon energy of 12 keV). Integrated scattering intensity of superlattice reflection (c) at (9/4, 5/4, 1/4) in $LaCoO_3$/LSAT(001) and (d) at (9/4, 7/4, 1/4) in $LaCoO_3$/STO(111).

recent studies have uncovered the emergence of long-period lattice modulation in the epitaxial films of $LaCoO_3$ and their Sr-doped analogs, which can be attributed to the spin-state ordering or oxygen vacancy ordering [21,28]. Given that the T_S is as low as 40 K, the spin state ordering is most plausible in the present case; it is reported that the diffusion of oxygen-ion and structural transformations irrelevant to the spin state crossover occur above 800 K in bulk $LaCoO_3$ [29].

To get insight into the spatial pattern of the spin-state ordering, we performed the resonant x-ray scattering. The anisotropy of the tensor of susceptibility is often resonantly enhanced due to the orbital polarization of d electrons and thus can be a powerful probe for the orbital ordering in transition metal compounds [30,31]. We note that the spectra show similar peak and dip structures at all the investigated azimuthal angles. Figure 4(e) shows the ψ dependence of scattering intensity of a peak at 7.74 keV. It is clear that the scattering intensity hardly depends on ψ, indicating that the local electronic symmetry of the Co $3d$ electron is nearly invariant against the rotation around the [111] axis. We also note that the lattice distortion, which violates the threefold rotational symmetry, could not be detected via the fundamental Bragg reflections within our experimental accuracy.

With these results in mind, we henceforth discuss the plausible models of spin-state ordering. Considering the ψ-independent resonant structure at the Co K edge, the involvement of IS state is not likely, since the Jahn-Teller distortion due to e_g-orbital polarization of IS state would break the rotational symmetry around the [111] axis. In this context, the spin-state disproportionation composed of LS state and HS state with reduced Jahn-Teller instability may be relevant. One plausible model is shown in Fig. 5(b); the HS-state sites align in every six sites along the [111] direction in the matrix of LS state with the ferromagnetic spin ordering. For clarity, we also show the schematic view of the crystal structure of bulk $LaCoO_3$ with the rhombohedral symmetry in Fig. 5(a). Here, we assumed that the lowest-energy state is $J_{\rm eff} = 1$ triplet, taking into account the moderate spin-orbit coupling under the weak trigonal crystal field (the compressive lattice distortion along the [111] direction) [32]. In terms of the magnetic structure, this model yields the net magnetization about 0.57 μ_B/Co, which is nearly comparable with the observed saturated magnetization; here we assumed that the local magnetic moment of HS state is 3.4 μ_B [7,10]. One other possible model is the spin-state disproportionation composed of LS-state sites and two inequivalent HS-state sites. In Fig. 5(c), we show two examples: the HS-state sites with inequivalent valence state ($Co^{(3-\delta)+}$ and Co^{3+}) or those with inequivalent hybridization with LS state ($\alpha_1|{\rm HS}\rangle + \beta_1|{\rm LS}\rangle$ and $\alpha_2|{\rm HS}\rangle + \beta_2|{\rm LS}\rangle$ with $\alpha_1 \neq \alpha_2$ and $\beta_1 \neq \beta_2$) [13]. By assuming that the local moments of both HS-state sites are approximately 3.4 μ_B, the net magnetization is estimated to be around 1.1 μ_B/Co, which is roughly consistent with the observed saturated magnetization.

Finally, we note that these possible models of spin-state ordering for $LaCoO_3$/LSAT(111) are distinct from that for $LaCoO_3$/LSAT(110) [22], in which a moderate epitaxial strain about ~1% is applied in the (110) crystal orientation. To clarify the role of magnitude and direction of epitaxial strain on the spin-state orderings, we have also investigated the spin-state ordering for $LaCoO_3$/LSAT(001) and $LaCoO_3$/STO(111), in which the epitaxial strain more than 1% is applied in the (001) and (111) crystal orientations, respectively. Figures 6(a) and 6(b) show typical profiles of superlattice reflection in these systems. In both systems, we have identified superlattice reflections characterized by $q = (1/4, 1/4, 1/4)$, which is the

same as the case of $LaCoO_3$/LSAT(110) [22]. The scattering intensities are plotted as a function of temperature in Figs. 6(c) and 6(d). From the threshold of scattering intensity, the transition temperature of spin-state ordering is estimated to be about 145 K for $LaCoO_3$/LSAT(001) and about 120 K for $LaCoO_3$/STO(111). These results suggest that the pattern of spin-state ordering is mainly governed by the magnitude of epitaxial strain rather than by its direction. It could be concluded in a previous study [22] that the IS and/or HS state are realized even at low temperatures in $LaCoO_3$/LSAT(110), while keeping a Mott insulating state. There has been extensive discussion on the plausible model for the thermally- or strain-induced spin-state transition in this system. One possible model is spin-state disproportionation composed of LS and HS state, in which the LS- and HS-state sites spatially coexist with each other. Another one is the uniform IS state accompanying the ordering of active e_g orbitals. More recently, complex spin-state disproportionation composed of all the LS, IS, and HS states has also been proposed [12,33,34]. While the assignment of spin-state ordering is still unsettled, we have exemplified one of the plausible spin-state disproportionation models composed of the LS and HS states with t_{2g}-orbital ordering in Fig. 5(d). This is in contrast with the spin-state ordering for $LaCoO_3$/LSAT(111), in which the HS-state sites are dilutely populated in the matrix of LS-state sites. Indeed, the spectral shape of Co-O phonons for $LaCoO_3$/LSAT(110) is quite different from that for $LaCoO_3$/LSAT(111) as shown in Fig. 4(d). On the basis of these results, we summarize the evolution of spin-state ordering in Fig. 1(b); the change in the population or character of spin state appears to cause the strain-induced variation of the magnetic ordering in a series of epitaxial thin films of $LaCoO_3$. These results suggest that the epitaxial strain is a powerful tool to tune the spin state and magnetic ordering in this canonical spin-crossover material, whereas it has already been established that the modification of crystal structure gives rise to a variety of spin-state ordering in other classes of cobalt oxides such as $YBaCoO_{5.5}$, Sr_2CoO_3Cl, and other ordered perovskites [35–37].

IV. CONCLUSION

In summary, we have investigated the lattice distortion coupled to the Co 3*d* spin-state ordering in epitaxial thin films of perovskite $LaCoO_3$. In the system with weak tensile strain of about 0.5%, we have found the long-period lattice distortion with the modulation vector $q = (1/6,1/6,1/6)$ at 40 K, followed by a ferromagnetic transition at 24 K. Combined with the results of resonant x-ray scattering at the Co *K* edge and infrared phonon anomaly, we propose that the ordering of high-spin-state sites in the matrix of low-spin-state sites is responsible for the ferromagnetic ordering. Alternatively, in systems with the tensile strain exceeding 1%, irrespective of the direction of epitaxial strain, we have identified the lattice distortion characterized by $q = (1/4,1/4,1/4)$, which can be interpreted as the spin-state ordering composed of the majority spin states with IS or HS state. The change in the population of IS- or HS-state sites may give rise to the strain-induced switching of spin-state ordering and resultant magnetism in this canonical correlated spin-state crossover material.

ACKNOWLEDGMENTS

This work was partly supported bya Grant-In-Aid for Science Research (Grant Nos. 24224009 and 26610097) from the MEXT, Japan and by Murata Funding by Funding Program for World-Leading Innovation R&D on Science and Technology (FIRST) on “Quantum Science on Strong-Correlation.”

[1] O. Kahn and C. Jay. Martinez, Science **279**, 44 (1998).
[2] A. Bousseksou, G. Molnar, J. AntonioReal, and K. Tanaka, Coord. Chem. Rev. **251**, 1822 (2007).
[3] P. M. Raccah and J. B. Goodenough, Phys. Rev. **155**, 932 (1967).
[4] V. G. Bhide, D. S. Rajoria, G. R. Rao, and C. N. R. Rao, Phys. Rev. B **6**, 1021 (1972).
[5] M. A. Korotin, S. Y. Ezhov, I. V. Solovyev, V. I. Anisimov, D. I. Khomskii, and G. A. Sawatzky, Phys. Rev. B **54**, 5309 (1996).
[6] C. Zobel, M. Kriener, D. Bruns, J. Baier, M. Gruninger, T. Lorenz, P. Reutler, and A. Revcolevschi, Phys. Rev. B **66**, 020402(R) (2002).
[7] S. Noguchi, S. Kawamata, K. Okuda, H. Nojiri, and M. Motokawa, Phys. Rev. B **66**, 094404 (2002).
[8] Z. Ropka and R. J. Radwanski, Phys. Rev. B **67**, 172401 (2003).
[9] K. Knizek, Z. Jirák, J. Hejtmánek, M. Veverka, M. Maryško, G. Maris, and T. T. M. Palstra, Eur. Phys. J. B **47**, 213 (2005).
[10] A. Podlesnyak, S. Streule, J. Mesot, M. Medarde, E. Pomjakushina, K. Conder, A. Tanaka, M. W. Haverkort, and D. I. Khomskii, Phys. Rev. Lett. **97**, 247208 (2006).
[11] M. W. Haverkort *et al.*, Phys. Rev. Lett. **97**, 176405 (2006).
[12] K. Knizek, Z. Jirak, J. Hejtmanek, P. Novak, and W. Ku, Phys. Rev. B. **79**, 014430 (2009).
[13] J. Kunes and V. Krapek, Phys. Rev. Lett. **106**, 256401 (2011).
[14] A. Doi, J. Fujioka, T. Fukuda, S. Tsutsui, D. Okuyama, Y. Taguchi, T. Arima, A. Q. R. Baron, and Y. Tokura, Phys. Rev. B **90**, 081109(R) (2014).
[15] D. Fuchs, C. Pinta, T. Schwarz, P. Schweiss, P. Nagel, S. Schuppler, R. Schneider, M. Merz, G. Roth, and H. v. Löhneysen, Phys. Rev. B **75**, 144402 (2007).
[16] J. W. Freeland, J. X. Ma, and J. Shi, Appl. Phys. Lett. **93**, 212501 (2008).
[17] V. V. Mehta, M. Liberati, F. J. Wong, R. V. Chopdekar, E. Arenholz, and Y. Suzuki, J. Appl. Phys. **105**, 07E503 (2009).
[18] A. D. Rata, A. Herklotz, L. Schultz, and K. Dorr, Eur. Phys. J. B **76**, 215 (2010).
[19] J. M. Rondinelli and N. A. Spaldin, Phys. Rev. B **79**, 054409 (2009).
[20] H. Hsu, P. Blaha, and R. M. Wentzcovitch, Phys. Rev. B **85**, 140404(R) (2012).
[21] W. S. Choi, J.-H. Kwon, H. Jeen, J. E. Hamann-Borrero, A. Radi, S. Macke, R. Sutarto, F. He, G. A. Sawatzky, V. Hinkov, M. Kim, and H. N. Lee, Nano Lett. **12**, 4966 (2012).

[22] J. Fujioka, Y. Yamasaki, H. Nakao, R. Kumai, Y. Murakami, M. Nakamura, M. Kawasaki, and Y. Tokura, Phys. Rev. Lett. **111**, 027206 (2013).

[23] Y. Konishi, Z. Fang, M. Izumi, T. Manako, M. Kasai, H. Kuwahara, M. Kawasaki, K. Terakura, and Y. Tokura, J. Phys. Soc. Jpn. **68**, 3790 (1999).

[24] K. Okazaki, S. Sugai, Y. Muraoka, and Z. Hiroi, Phys. Rev. B **73**, 165116 (2006).

[25] D. P. Kozlenko, N. O. Golosova, Z. Jirák, L. S. Dubrovinsky, B. N. Savenko, M. G. Tucker, Y. Le Godec, and V. P. Glazkov, Phys. Rev. B **75**, 064422 (2007).

[26] M. M. Altarawneh, G.-W. Chern, N. Harrison, C. D. Batista, A. Uchida, M. Jaime, D. G. Rickel, S. A. Crooker, C. H. Mielke, J. B. Betts, J. F. Mitchell, and M. J. R. Hoch, Phys. Rev. Lett. **109**, 037201 (2012).

[27] S. Yamaguchi, Y. Okimoto, and Y. Tokura, Phys. Rev. B, **55**, R8666(R) (1997).

[28] J. Gazquez, W. Luo, M. P. Oxley, M. Prange, M. A. Torija, M. Sharma, C. Leighton, S. T. Pantelides, S. J. Pennycook, and M. Varela, Nano Lett. **11**, 973 (2011).

[29] P. G. Radaelli and S. W. Cheong, Phys. Rev. B **66**, 094408 (2002).

[30] Y. Murakami, J. P. Hill, D. Gibbs, M. Blume, I. Koyama, M. Tanaka, H. Kawata, T. Arima, Y. Tokura, K. Hirota, and Y. Endoh, Phys. Rev. Lett. **81**, 582 (1998).

[31] M. v. Zimmermann, J. P. Hill, D. Gibbs, M. Blume, D. Casa, B. Keimer, Y. Murakami, Y. Tomioka, and Y. Tokura, Phys. Rev. Lett. **83**, 4872 (1999).

[32] It is argued that the lowest energy state of high spin configuration is the nondegenerate state, which has approximately the character of the $|j_z = 0\rangle$ state in Refs. [7]online and [8]online. Although the exact character of the orbital state could not be specified in the present system, the anisotropy around the [111] axis would be much smaller than the possible Jahn-Teller distortion due to the IS state. To derive a more accurate picture of orbital state, we have to take into account the intersite exchange interaction in addition to the crystal field and spin-orbit coupling in a more quantitative manner.

[33] V. Křápek, P. Novák, J. Kuneš, D. Novoselov, Dm. M. Korotin, and V. I. Anisimov, Phys. Rev. B **86**, 195104 (2012).

[34] G. Zhang, E. Gorelov, E. Koch, and E. Pavarini, Phys. Rev. B **86**, 184413 (2012).

[35] C. S. Knee, D. J. Price, M. R. Lees, and M. T. Weller, Phys. Rev. B **68**, 174407 (2003).

[36] D. D. Khalyavin, D. N. Argyriou, U. Amann, A. A. Yaremchenko, and V. V. Kharton, Phys. Rev. B **75**, 134407 (2007).

[37] S. Ishiwata, W. Kobayashi, I. Terasaki, K. Kato, and M. Takata, Phys. Rev. B **75**, 220406(R) (2007).